Available online at www.sciencedirect.com
ScienceDirect
Journal of Molecular Catalysis A: Chemical 261 (2007) 276–281
JOURNAL OF MOLECULAR CATALYSIS A: CHEMICAL
www.elsevier.com/locate/molcata

Role and effect of molybdenum on the performance of Ni-Mo/γ-Al_2O_3 catalysts in the hydrogen production by auto-thermal reforming of ethanol

Min Hye Youn [a], Jeong Gil Seo [a], Pil Kim [b], In Kyu Song [a,*]

[a] *School of Chemical and Biological Engineering, Research Center for Energy Conversion and Storage, Seoul National University, Shinlim-dong, Kwanak-ku, Seoul 151-744, South Korea*
[b] *School of Environmental and Chemical Engineering, Chonbuk National University, Jeonju, Jeonbuk 561-756, South Korea*

Received 19 July 2006; accepted 10 August 2006
Available online 12 September 2006

Abstract

Bimetallic Ni-Mo/γ-Al_2O_3 catalysts (Ni20Mo*X*, Ni = 20 wt.%, *X* = 0, 3, 5, 7, and 9 wt.%) with different Mo contents were prepared using a co-impregnation method. The role and effect of Mo on the catalytic performance of the Ni-Mo/γ-Al_2O_3 catalysts in the auto-thermal reforming of ethanol was examined. It was found that the addition of Mo up to 7 wt.% decreased the interaction between the Ni species and the alumina support, increasing the reducibility of Ni species. On the other hand, the Ni20Mo9 catalyst was less effective in hydrogen production than the Ni20Mo7 catalyst due to the formation of bulky $NiMoO_4$ in the Ni20Mo9 catalyst. It was also revealed that Mo species served as a barrier for preventing the growth of Ni particles, leading to the formation of highly dispersed Ni-Mo/γ-Al_2O_3 catalysts. In the auto-thermal reforming of ethanol, bimetallic Ni20Mo*X* catalysts (*X* = 3, 5, and 7 wt.%) catalysts exhibited a higher catalytic performance than the monometallic Ni20 catalyst. Among the catalysts tested, the Ni20Mo5 catalyst showed the best catalytic performance. However, addition of excess Mo (9 wt.%) decreased the catalytic performance of the bimetallic supported catalyst, resulting from both poor reducibility of Ni species and coverage of Ni sites by MoO_X species. It was also observed that the Ni20 catalyst experienced a severe catalyst deactivation due to coke deposition on the catalyst surface during the catalytic reaction.

Keywords: Ni-Mo/γ-Al_2O_3 catalysts; Hydrogen production; Deactivation; Auto-thermal reforming of ethanol; Metal–support interaction; Reducibility

1. Introduction

The clean, renewable, and non-polluting nature of hydrogen has attracted considerable attention for its use as an alternative energy source. However, abundant hydrogen is not found in nature but needs be produced from water or organic compounds [1,2]. Therefore, feasible routes for hydrogen production are necessary for the practical use of hydrogen.

Most hydrogen currently used in industry is produced by steam or auto-thermal reforming of light hydrocarbons such as methanol, ethanol, and natural gas [3–7]. In particular, light alcohols are a promising source for hydrogen production because they can be easily handled and are widely distributed over the world. Although methanol is commonly used as a hydrogen source, ethanol has advantages as an alternative hydrogen source on account of its low toxicity, high volumetric energy density, and availability [8–18].

The yield of hydrogen produced by the auto-thermal reforming of ethanol strongly depends on the catalyst system. Although a high yield of hydrogen can be achieved over noble metal-based catalysts such as Rh/Al_2O_3 at low temperatures, the high cost of noble metals limits the practical applications of noble metal-based catalyst systems in the hydrogen production by the auto-thermal reforming of ethanol [14–16]. It has been reported that non-noble metal-based catalysts also show a relatively high catalytic performance in the auto-thermal reforming of ethanol [17,18]. In particular, the intrinsic high activity and low cost of Ni has made it a promising catalyst [17]. However, one of the major problems in the application of Ni catalyst is the catalyst deactivation caused by carbon deposition on the catalyst surface. Therefore, many studies [16–18] have been carried out to improve the stability of Ni catalyst by using second metals such as Rh, Cu, and Co. It is

* Corresponding author. Tel.: +82 2 880 9227; fax: +82 2 888 7295.
E-mail address: inksong@snu.ac.kr (I.K. Song).

1381-1169/$ – see front matter © 2006 Elsevier B.V. All rights reserved.
doi:10.1016/j.molcata.2006.08.030

believed that these second metals suppress the coke deposition by forming a Ni–metal alloy or by modifying the Ni ensemble [16–18].

It was reported that a Ni catalyst modified with small amount of Mo showed stable catalytic performance in the steam reforming of *n*-butane because the addition of Mo not only decreases the rate of coking but also extends the induction period of coking [19]. Although the effect of Mo addition on the catalytic performance of Ni has been investigated in the steam reforming of hydrocarbons such as methane [20] and *n*-butane [21], no attempt has been made in the hydrogen production by the auto-thermal reforming of ethanol.

In this study, a series of Ni-Mo/γ-Al_2O_3 catalysts with various Mo contents were prepared using a co-impregnation method. These catalysts were applied to the hydrogen production by the auto-thermal reforming of ethanol in a continuous flow fixed-bed reactor. The prepared catalysts were characterized by X-ray diffraction (XRD), transmission electron microscopy (TEM), and temperature-programmed reduction (TPR) measurements. The role and effect of Mo on the catalytic performance of Ni-Mo/γ-Al_2O_3 in the auto-thermal reforming of ethanol was investigated.

2. Experimental

2.1. Preparation of Ni-Mo/γ-Al_2O_3 catalyst

The Ni-Mo/γ-Al_2O_3 catalysts (Ni/γ-Al_2O_3 catalysts containing Mo as a second metal) were prepared by co-impregnating the appropriate amounts of nickel ($Ni(NO_3)_2{\cdot}6H_2O$, Aldrich) and molybdenum precursors ($(NH_4)_6\ Mo_7O_{24}{\cdot}4H_2O$, Aldrich) onto γ-$Al_2O_3$ (Degussa). The co-impregnated catalyst samples were dried at 120 °C, and calcined at 900 °C for 8 h. In a series of Ni-Mo/γ-Al_2O_3 catalysts, the Ni loading on γ-Al_2O_3 was fixed at 20 wt.% while the Mo loadings were varied from 0 to 9 wt.%. The prepared Ni-Mo/γ-Al_2O_3 catalysts were denoted as Ni20Mo*X* (*X* = 0, 3, 5, 7, and 9). For example, the Ni20Mo5 catalyst represents 20 wt.% Ni and 5 wt.% Mo were loaded on γ-Al_2O_3.

2.2. Characterization

The crystalline phases of the calcined and reduced catalysts were examined by XRD (M18XHF-SRA, MAC Science Co.) using Cu Kα radiation (λ = 1.54056 Å) operated at 50 kV and 100 mA. The size and location of the metal particles on the catalyst surface were confirmed by transmission electron microscopy (TEM, Joel, JXA-8900R) using an ultrasonically dispersed catalyst sample (in ethanol) deposited on a carbon grid. The reducibility of the catalysts was examined by temperature-programmed reduction (TPR) measurements in a conventional flow system with a moisture trap connected to a thermal conductivity detector (TCD) at temperatures ranging from room temperature to 1000 °C with a ramping rate of 5 °C/min. For the TPR measurements, a mixed stream of H_2 (2 ml/min) and N_2 (20 ml/min) was used for 0.1 g of the catalyst sample.

2.3. Auto-thermal reforming of ethanol

The auto-thermal reforming of ethanol was carried out in a continuous flow fixed-bed reactor at atmospheric pressure. Each calcined catalyst (50 mg) was charged into a tubular quartz reactor, and then it was reduced with a mixed stream of H_2 (10 ml/min) and N_2 (30 ml/min) at 700 °C for 3 h. Ethanol and water were sufficient vaporized by passing a pre-heating zone and fed into the reactor continuously together with a N_2 carrier (30 ml/min). The feed ratios of H_2O/EtOH and O_2/EtOH were fixed at 2.0 and 0.8, respectively. The contact time was maintained at 175 g-catalyst·min/EtOH-mole, and the catalytic reaction was carried out at 550 °C. The reaction products were periodically sampled and analyzed using an on-line gas chromatograph (Younglin, ACME 6000) equipped with two TCDs.

3. Results and discussion

3.1. Crystalline phases of Ni20MoX (X = 0, 3, 5, 7, and 9)

Fig. 1 shows the XRD patterns of γ-Al_2O_3 and Ni20Mo*X* (*X* = 0, 3, 5, 7, and 9) catalysts calcined at 900 °C for 8 h. No peaks related to nickel oxide or molybdenum oxide were found in the Ni20Mo*X* (*X* = 3, 5, and 7) catalysts, and only broad peaks corresponding to γ-Al_2O_3 were observed. This indicates that the metal oxides were highly dispersed on the support [19]. On the other hand, the Ni20Mo9 catalyst showed both MoO_3 (JCPDS 47-1081) and $NiMoO_4$ (JCPDS 33-098) phases. It should be noted that the (4 4 0) diffraction peak of γ-Al_2O_3 shifted to a lower angle when the metal species were loaded on the γ-Al_2O_3. This suggests that the lattice of γ-Al_2O_3 expanded as a result of Ni incorporation due to the strong interaction between the Ni species and γ-Al_2O_3 [22]. The Ni20Mo*X* (*X* = 3, 5, 7, and 9) catalysts showed a smaller degree of lattice expansion than the Ni20 catalyst. The alumina lattice in the Ni20Mo*X* (*X* = 3, 5, 7, and 9) catalysts was decreased with increasing Mo content. It is likely that the presence of Mo species impedes the incorporation of Ni species into the alumina lattice, leading to less lattice expansion in the bimetallic Ni20Mo*X* (*X* = 3, 5, 7, and 9) cata-

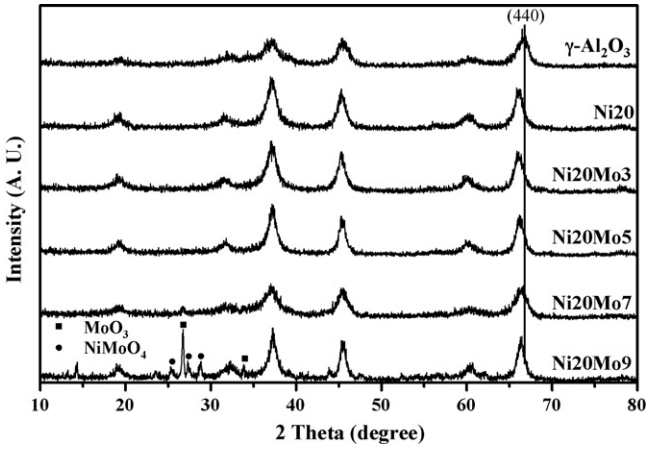

Fig. 1. XRD patterns of γ-Al_2O_3 and Ni20Mo*X* (*X* = 0, 3, 5, 7, and 9) catalysts calcined at 900 °C for 8 h.

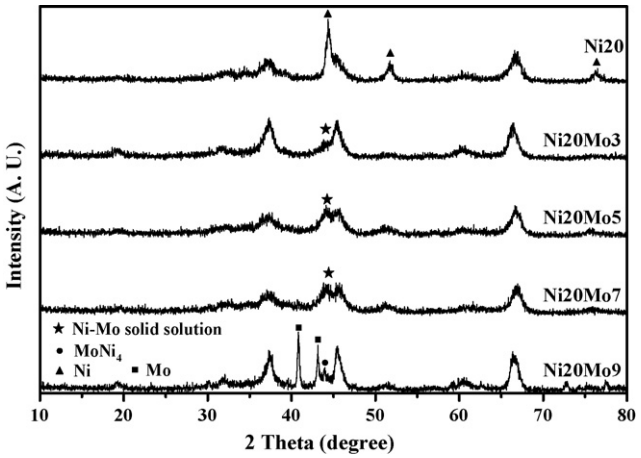

Fig. 2. XRD patterns of Ni20Mo*X* (*X* = 0, 3, 5, 7, and 9) catalysts reduced at 700 °C for 3 h.

lysts than in the Ni20 catalyst. This means that the presence of Mo species reduces the interaction between the Ni species and γ-Al_2O_3, which in turn decreases the amount of Ni incorporated into the γ-Al_2O_3 lattice.

Fig. 2 shows the XRD patterns of Ni20Mo*X* (*X* = 0, 3, 5, 7, and 9) catalysts reduced at 700 °C for 3 h. The reduced Ni20 catalyst showed relatively narrow XRD peaks corresponding to metallic Ni, indicating the formation of large Ni particles after reduction. On the other hand, the Ni20Mo*X* (*X* = 3, 5, 7, and 9) catalysts showed somewhat different XRD patterns from the Ni20 catalyst. The XRD peaks for metallic Ni disappeared upon the addition of Mo. Instead, a broad peak resulting from the formation of a Ni-Mo solid solution with a Ni-rich structure was observed in the Ni20Mo*X* (*X* = 3, 5, and 7) catalysts [19]. However, the Ni20Mo9 catalyst showed the characteristics peaks for both metallic Mo (JCPDS 42-1120) and inter-metallic $MoNi_4$ (JCPDS 03-1036) that is known to be formed by the reduction of $NiMoO_4$ [23]. It is interesting that the XRD peaks for metallic Ni were not developed in the reduced Ni20Mo*X* (*X* = 3, 5, 7, and 9) catalysts, even though narrow XRD peaks for metallic Ni should appear after the reduction of bimetallic Ni20Mo*X* catalysts because the calcined Ni20Mo*X* (*X* = 3, 5, 7, and 9) retained a weak interaction between Ni species and γ-Al_2O_3 compared to the calcined Ni20 (Fig. 1). It is believed that the highly dispersed Mo species on γ-Al_2O_3 prevented the growth of metallic Ni particles through the formation of a Ni-Mo solid solution in the case of Ni20Mo*X* (*X* = 3, 5, and 7) [19] or through the formation of an inter-metallic compound such as $MoNi_4$ in the case of Ni20Mo9 [23]. This result was evidenced by TEM images of the reduced catalysts.

Fig. 3 shows the TEM images of Ni20 and Ni20Mo5 catalysts reduced at 700 °C for 3 h. Compared with the Ni20 catalyst, the Ni20Mo5 catalyst had finely dispersed metallic species on γ-Al_2O_3, which is well consistent with the XRD results of the reduced catalysts (Fig. 2).

3.2. Reducibility of Ni20MoX (X = 0, 3, 5, 7, and 9)

TPR measurements were carried out to investigate the reducibility of Ni20Mo*X* catalysts and to see the interaction between the metal species and γ-Al_2O_3. The reduction profiles of the supported Ni catalysts are dependent on the interaction between the Ni species and γ-Al_2O_3 [22–24]. For example, unsupported NiO is reduced at approximately 400 °C, while the reduction band for Ni species supported on γ-Al_2O_3 appears at 500–700 °C. In particular, Ni species in the lattice of nickel aluminate, which are known to strongly interact with γ-Al_2O_3, are reduced at approximately 800 °C.

As shown in Fig. 4, the reduction profiles of the Ni20Mo*X* (*X* = 0, 3, 5, 7, and 9) catalysts varied depending on the amount of Mo added. The monometallic Ni20 catalyst showed a broad reduction band with the highest reduction peak temperature,

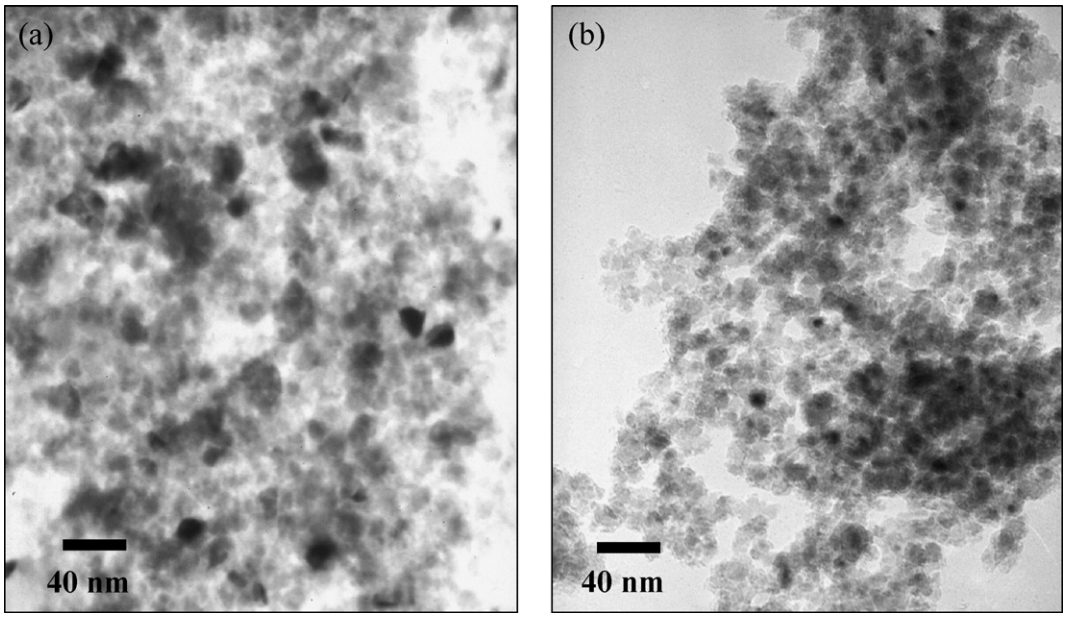

Fig. 3. TEM images of (a) Ni20 and (b) Ni20Mo5 catalysts reduced at 700 °C for 3 h.

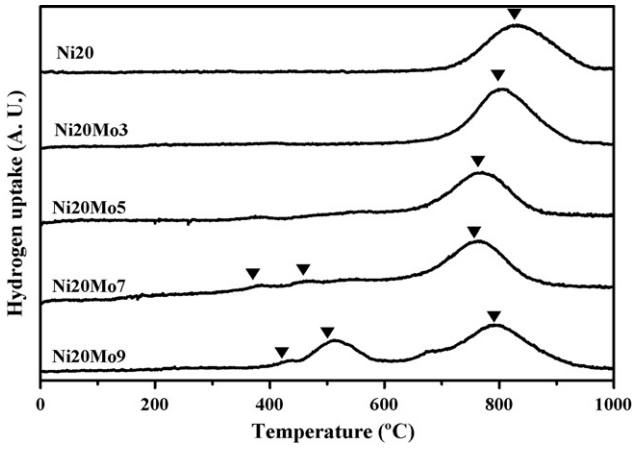

Fig. 4. TPR patterns of Ni20MoX (X = 0, 3, 5, 7, and 9) catalysts.

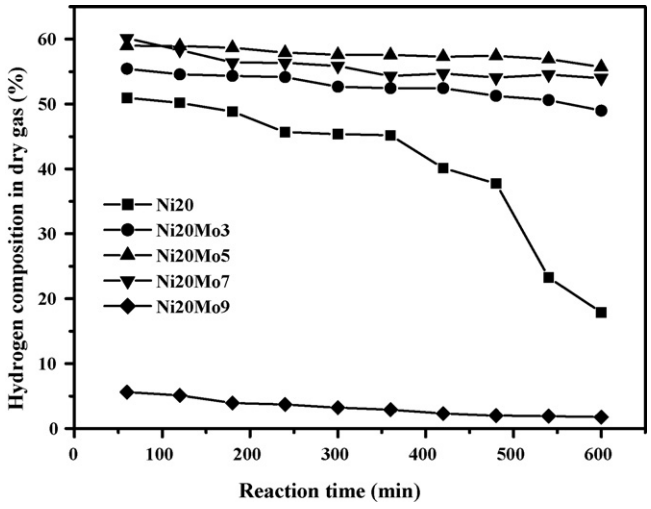

Fig. 5. Hydrogen composition in dry gas with time on stream in the auto-thermal reforming of ethanol over Ni20MoX (X = 0, 3, 5, 7, and 9) catalysts at 550 °C.

while the reduction bands of the bimetallic supported catalysts shifted to a lower temperature with increasing Mo content except for the Ni20Mo9 catalyst. This is somewhat contradictory to earlier observations [19,25], in which bimetallic Ni-Mo catalyst was reported to be less reducible than the monometallic Ni catalyst. It was also reported that the reduction pattern of the bimetallic Ni-Mo catalyst depended on several factors such as the catalyst preparation method and the catalyst pretreatment conditions [19,23,25]. The bimetallic Ni-Mo catalysts in previous works [19,23,25] were prepared using sequential impregnation, while those in this study were prepared using a co-impregnation method. Therefore, it is believed that the catalyst preparation method is responsible for the different reduction patterns of our catalysts compared with the bimetallic catalysts reported in the literatures [19,23,25].

Besides the main broad reduction band, both Ni20Mo7 and Ni20Mo9 showed additional reduction bands at the low temperature region of 350–600 °C, which were assigned to the reduction of molybdenum oxide with various oxidation states [19]. The reduction band for the Mo species was barely observed in both Ni20Mo3 and Ni20Mo5 because of the relatively low Mo contents in these catalysts. One additional reduction peak in the Ni20Mo9 catalyst appearing at approximately 500 °C was quite strong, which was attributed to the reduction of MoO_3 to metallic Mo [19], as evidenced by XRD (Figs. 1 and 2). Interestingly, the peak temperature of the main broad reduction band of the supported catalysts, with the exception of Ni20Mo9, showed a similar trend to the degree of lattice expansion of alumina shown by XRD. This demonstrates that the reduction of Ni species is strongly affected by the interaction between the Ni species and γ-Al_2O_3. On the other hand, the Ni20Mo9 catalyst showed a higher peak temperature for the main reduction band than the Ni20Mo7 even though there was less expansion of the alumina lattice in the former catalyst than in the latter. The relatively poor reducibility of Ni20Mo9 might be due to the formation of a bulky $NiMoO_4$ phase (Fig. 1). It is believed that the Ni species were decorated by MoO_X species, leading to the poor reducibility of Ni20Mo9 catalyst [26–28].

3.3. Auto-thermal reforming of ethanol over Ni20MoX (X = 0, 3, 5, 7, and 9)

All the catalysts tested in this study showed almost complete conversion of ethanol at 550 °C, while the product distributions over Ni20MoX (X = 0, 3, 5, 7, and 9) catalysts were different depending on the Mo content. Fig. 5 shows the hydrogen composition in dry gas with time on stream in the auto-thermal reforming of ethanol over Ni20MoX (X = 0, 3, 5, 7, and 9) catalysts at 550 °C. The bimetallic supported catalysts except for Ni20Mo9 showed a higher catalytic performance than the monometallic Ni20 catalyst. There are two possible reasons for the enhanced catalytic performance of Ni20MoX (X = 3, 5, and 7). One is that both active surface area and reducibility of these catalysts were increased by the addition of Mo, as confirmed by XRD and TEM measurements. The other reason is that the electronic structure of Ni was favorably modified for the reaction, which is in good agreement with previous studies [26–28] reporting that electron transfer from MoO_X to active Ni species improved the catalytic activity. Among the catalyst tested, the Ni20Mo5 showed the best catalytic performance. The catalytic performance was decreased in the order of Ni20Mo5 > Ni20Mo7 > Ni20Mo3 > Ni20 > Ni20Mo9. Although fundamental reason for the low catalytic performance of Ni20Mo9 is unclear, it is believed that the decoration of Ni sites by MoO_X species in this catalyst resulted in the low catalytic performance, as mentioned earlier [26–28]. In addition, the poor reducibility of the Ni20Mo9 catalyst is also responsible for its low catalytic performance. It should be noted that the Ni20 catalyst experienced a severe catalyst deactivation, unlike the Ni20MoX (X = 3, 5, 7, and 9) catalysts.

Fig. 6 shows the by-product distribution over Ni20 and Ni20Mo5 catalysts with time on stream in the auto-thermal reforming of ethanol at 550 °C. The compositions of CO, CO_2, and CH_4 over the Ni20Mo5 catalyst changed slightly with the time on stream, while negligible amounts of C_2 compounds such as C_2H_4 and CH_3CHO were formed over the Ni20Mo5 catalyst.

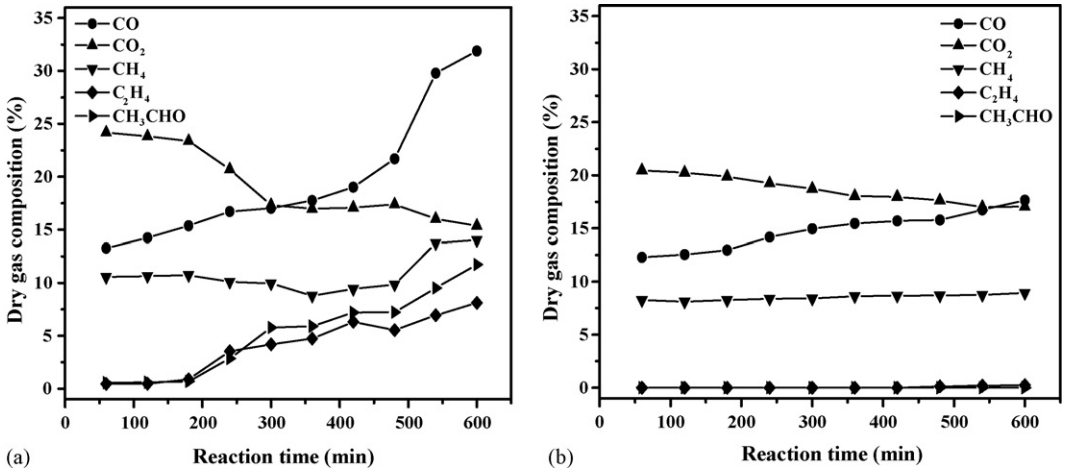

Fig. 6. By-product distribution over (a) Ni20 and (b) Ni20Mo5 catalysts with time on stream in the auto-thermal reforming of ethanol at 550 °C.

However, the by-product compositions over the Ni20 catalyst were drastically changed with the time on stream. It should be noted that the composition of C_2 compounds such as C_2H_4 and CH_3CHO over the Ni20 was much higher than that over the Ni20Mo5 catalyst. In addition, the increase in the CO composition at the expense of CO_2 was remarkable over the Ni20 catalyst. This suggests that the Ni20 catalyst becomes deactivated in the C–C bond cleavage ($CH_3CHO + H_2O + O_2 \rightarrow 2CO_2 + 3H_2$, $C_2H_4 + 2H_2O \rightarrow CO_2 + CH_4 + 2H_2$) [29–31]. It is widely accepted that the deactivation of the Ni catalyst in the steam reforming of ethanol is mainly due to carbon deposition on the catalyst surface [32]. In this catalyst system, a large amount of coke was deposited on the surface of the Ni20 catalyst (the amount of carbon deposition after a 10 h reaction was 76.3%) during the auto-thermal reforming of ethanol, resulting in a loss of catalytic activity for C–C bond cleavage. On the other hand, judging from the stable catalytic performance and extremely low selectivity for C_2 compounds over the Ni20Mo5 catalyst (carbon deposition after 10 h reaction was 27.9%), it is believed that the Mo species incorporated with the Ni catalyst suppress coke formation. As mentioned earlier, Ni catalyst modified with a small amount of Mo shows strong resistance toward coke formation because Mo species not only decrease the coking rate but also prolong the induction period of coke formation [19]. As evidenced by XRD (Fig. 2) and TEM (Fig. 3), it was also revealed that the highly dispersed Mo species served as a barrier for preventing the growth of Ni particles. This is another reason for the low rate of coke deposition on the bimetallic Ni20Mo5 catalyst. This result is consistent with previous studies [33–35] reporting that the rate of coke deposition increased with increasing particle size of the Ni catalyst.

4. Conclusions

Ni20Mo*X* (*X* = 0, 3, 5, 7, and 9) catalysts with different Mo contents were prepared using a co-impregnation method, and they were applied to the hydrogen production by auto-thermal reforming of ethanol. The role and effect of Mo on the catalytic property and catalytic performance of Ni20Mo*X* was examined. It was found that the presence of Mo species impeded the incorporation of Ni species into the lattice of alumina, leading to less lattice expansion of alumina in the Ni20Mo*X* catalysts. This resulted in a weak metal–support interaction, and consequently, increased the reducibility of the supported catalysts. The Ni20Mo9 catalyst was less effective in hydrogen production than the Ni20Mo7 catalyst due to the formation of bulky $NiMoO_4$. It was also observed that the Mo species served as a barrier for preventing the growth of Ni particles, leading to the formation of highly dispersed Ni-Mo/γ-Al_2O_3 catalysts. In the auto-thermal reforming of ethanol, the bimetallic Ni20Mo*X* (*X* = 3, 5 and 7) catalysts except for Ni20Mo9 showed a higher catalytic performance than the monometallic Ni20 catalyst, because the presence of small amount of Mo was effective in suppressing coke formation and in promoting the catalytic activity of Ni catalyst for the cleavage of the C–C bond. Among the catalysts tested, the Ni20Mo5 catalyst showed the best catalytic performance in the auto-thermal reforming of ethanol. However, the addition of excess Mo (in case of Ni20Mo9) decreased the catalytic performance, as a result of both poor reducibility of Ni species and coverage of Ni sites by MoO_X species. The Ni20 catalyst experienced a severe catalyst deactivation as a result of coke deposition on the catalyst surface and the subsequent loss of catalytic activity for the C–C bond cleavage.

Acknowledgement

This work was supported by KOSEF (Korea Science and Engineering Foundation) through the Research Center for Energy Conversion and Storage (R11-2002-102-00000-0).

References

[1] I. Narvàez, A. Orio, M.P. Aznar, J. Corella, Ind. Eng. Chem. Res. 35 (1996) 2110.
[2] C.D. Blasi, G. Sinorelli, G. Portoricco, Ind. Eng. Chem. Res. 38 (1999) 2571.
[3] P.D. Vaidya, A.E. Rodrigues, Chem. Eng. J. 117 (2006) 39.
[4] I. Fishtik, A. Alexander, R. Datta, D. Geana, Int. J. Hydro. Energy 25 (2000) 31.

[5] M. Asadullah, K. Tomishige, K. Fujimoto, Catal. Commun. 2 (2001) 63.
[6] S.J. Kong, J.H. Jun, K.J. Yoon, Korean J. Chem. Eng. 21 (2004) 793.
[7] R.M. Navarro, M.C. Álvarez-Galván, M.C. Sánchez-Sánchez, F. Rosa, J.L.G. Fierro, Appl. Catal. B 55 (2005) 229.
[8] J. Zhang, Y. Wang, R. Ma, D. Wu, Korean J. Chem. Eng. 20 (2003) 288.
[9] F. Aupretre, C. Descorme, D. Duprez, D. Casanave, D. Uzio, J. Catal. 233 (2005) 464.
[10] F. Aupretre, C. Descorme, D. Duprez, Catal. Commun. 3 (2002) 263.
[11] S. Cavallaro, V. Chiodo, S. Freni, N. Mondello, F. Frusteri, Appl. Catal. A 249 (2003) 119.
[12] A.N. Fatsikostas, X.E. Verykios, J. Catal. 225 (2004) 439.
[13] F. Frusteri, S. Freni, L. Spadaro, V. Chiodo, G. Bonura, S. Donato, S. Cavallaro, Catal. Commun. 5 (2004) 611.
[14] E. Vessellia, G. Comellia, R. Roseia, S. Freni, F. Frusteri, S. Cavallaro, Appl. Catal. A 281 (2005) 139.
[15] S. Cavallaro, V. Childo, A. Vita, S. Freni, J. Power Sources 123 (2003) 10.
[16] J. Kugai, V. Subramani, C. Song, M.H. Engelhard, Y.-H. Chin, J. Catal. 238 (2006) 430.
[17] V. Fierro, O. Akdim, H. Provendier, C. Mirodatos, J. Power Sources 145 (2005) 659.
[18] S. Velu, N. Satoh, C.S. Gopinath, K. Suauki, Catal. Lett. 82 (2002) 145.
[19] T. Borowiecki, W. Gac, A. Gotebiowski, Appl. Catal. A 270 (2004) 27.
[20] T. Borowiecki, A. Gotebiowski, B. Stasifiska, Appl. Catal. A 153 (1997) 141.
[21] T. Borowiecki, A. Gotębiowski, Catal. Lett. 25 (1994) 309.
[22] P. Kim, Y. Kim, H. Kim, I.K. Song, J. Yi, Appl. Catal. A 272 (2004) 157.
[23] M.A. Tsurov, P.V. Afanasiev, V.V. Lunin, Appl. Catal. A 105 (1993) 205.
[24] P. Kim, Y. Kim, C. Kim, H. Kim, Y. Park, J.H. Lee, I.K. Song, J. Yi, Catal. Lett. 89 (2003) 185.
[25] C.E. Quincoces, S.P. de Vargas, P. Grange, M.G. Gonzalez, Mater. Lett. 56 (2002) 698.
[26] A.E. Aksoylu, Z. Misirli, Z.I. Onsan, Appl. Catal. A 168 (1998) 385.
[27] A.E. Aksouly, Z.I. Onsan, Appl. Catal. A 168 (1998) 399.
[28] A.E. Aksouly, A.I. Isli, Z.I. Onsan, Appl. Catal. A 183 (1999) 357.
[29] F. Mariño, M. Boveri, G. Baronetti, M. Laborde, Int. J. Hydro. Energy 26 (2001) 665.
[30] F. Mariño, G. Baronetti, M. Jobbagy, M. Laborde, Appl. Catal. A 238 (2003) 41.
[31] F.J. Mariño, E.G. Cerrella, S. Duhalde, M. Jobbagy, M.A. Laborde, Int. J. Hydro. Energy 23 (1998) 1095.
[32] A.J. Akande, R.O. Idem, A.K. Dalai, Appl. Catal. A 287 (2005) 159.
[33] O.S. Joo, K.D. Jung, Bull. Kor. Chem. Soc. 23 (2002) 1149.
[34] J.-H. Lee, E.-G. Lee, O.-S. Joo, K.-D. Jung, Appl. Catal. A 269 (2004) 1.
[35] H.M. Swaan, C.C.H. Kroll, G.A. Martin, C. Mirodatos, Catal. Today 21 (1994) 571.